International Journal of Computer (IJC)
ISSN 2307-4523 (Print & Online)
https://ijcjournal.org/index.php/InternationalJournalOfComputer/index

Low Dimension Medical Images and Generative Deep Learning Models Can Help to Reduce X-Ray Radiation Exposure of Patients

Neha Vinayak [a], Divyansh Pandey [b], Shandar Ahmad [c*]

[a,b,c]*School of Computational and Integrative Sciences (SCIS), Jawaharlal Nehru University (JNU), New Delhi-110067, India*

[a]*Email: nehavinayak25@gmail.com*

[b]*Email: pdivyansh22@gmail.com*

[c]*Email: shandar@jnu.ac.in*

Abstract

Background: X-ray and other radiation-based diagnosis form a critical step in many clinical investigations, including early detection of diseases. Deep learning based methods to derive diagnosis from medical images have been shown to be highly accurate in this regard. However, the radiological images collected for this purpose continue to be guided by what is suitable for clinical practitioners to visually interpret them, ignoring the possibility that machines can detect patterns better than the human eye, making the high dimension images unnecessary. On the other hand, image analysis studies have primarily focused on classification accuracy, ignoring the diagnostic tradeoffs with radiation exposure.

Methods: Chest X-ray images from medical datasets have been modeled using EfficientNetB0 deep learning model by reducing the images to different pixel sizes: 1 x 1, 2 x 2, 4 x 4, 8 x 8, 16 x 16, 32 x 32, 64 x 64, 128 x 128, 224 x 224, 256 x 256 and 300 x 300 pixels. The effect of increasing image size on the predictive power of the model has been studied viz-a-viz the radiation exposure of the patient for collecting a chest X-ray image of that size.

Results: In this work, we show that reduced image sizes from the original X-ray images are capable of accurate diagnosis of medical conditions with little loss in predictive power and propose that potentially lower dimensions than what is needed for visual inspection may be sufficient for the purpose, thereby substantially reducing the risks associated with high radiation dosage, currently practiced for use of images by human interpretation. We also demonstrate how reduced images can be used to generate high dimension versions suitable for visual inspection with the help of generative super-resolution techniques (SRGAN) based on deep learning.

Received: 9/15/2024
Accepted: 11/15/2024
Published: 11/25/2024

---

* Corresponding author.

Conclusions: In summary this paper makes a case for low dimension collection of X-ray images, with accurate clinical outcomes and thereby addresses the issue of resolution versus diagnostic accuracy.

Keywords: Medical imaging; Medical image quality; Chest X-ray; X-ray image size; Radiation dosage; Radiation exposure.

1. Introduction

X-rays were first produced unknowingly by William Morgan in 1785 [1,2]. This new type of ray was discovered experimentally by Wilhelm Röntgen in 1895. He called the radiation "X" as they were not known before. The use of X-rays in medical diagnosis was discovered by Röntgen when he took a picture of his wife's hand on an X-ray photographic plate. Since then, X-rays have created medical imaging as a critical tool in non-invasive diagnosis of many disease conditions. This has made detection of diseases like covid-19 and pneumonia faster. During the covid-19 pandemic, when RT-PCR tests took several days to detect the disease, chest X-rays came to the rescue and helped in early diagnosis [3], thus preventing serious damage to the lungs of patients. X-rays are also used in a multitude of other medical scanning applications like CT scans, angiography, fluoroscopy etc. [4].

Some of these technologies expose human subjects to high radiation doses to produce better quality images. An issue of concern, therefore, is that of the increased use of imaging techniques and repeated exposure leading to DNA damage, cancer-causing mutations and birth defects and several other known and unknown side effects Reference [5,6]. These side effects have been separately investigated for example in the younger generation suffering from scoliosis [7] and in premature babies being treated in NICUs [8,9] who must undergo many X-ray scans as part of their treatment, putting them at high risk due to induced radiation. According to a study [10], pneumonia is a leading cause of mortality in children less than 5 years of age, which again is diagnosed by chest X-rays. In the past few years, Covid-19 has claimed millions of lives across the world and Chest X-ray has been used for its diagnosis, among other techniques. While diagnosing any disease using X-ray based methods, the effect of radiation exposure is seen to be proportional to increasing radiation dosage [4]. Repeated or high intensity dosage at early ages increases the risk of cancer due to radiation8, even though the risk is found to be lower at higher ages [11]. Among patients who undergo CT angiography at 40 years of age, 1 in 270 women and 1 in 600 men are found to develop cancer [12]. The risk of these scans performed for 20-year-olds is found to be twice as much, while for 60-year-olds, the risk is half.

Even though various safety standards are followed in performing X-rays-based diagnosis, repeated and unnecessarily high exposure poses many risks. Reducing this radiation further will make the process even safer, decreasing the risk to human life. When the body is exposed to X-rays, the radiation either passes through the body unabsorbed or is absorbed by the body organs. The unabsorbed part of the radiation falls on the film to create the X-ray image while the other part, which is absorbed by the body is harmful. The latter is measured as the radiation dosage [13]. In this study, we work towards providing a lower radiation dosage framework for automated diagnosis from X-ray images by optimizing best image sizes without loss of diagnostic value.

Image Quality Vs Radiation Dosage: The quality of an image can be measured as the number of pixels

forming the image. According to a study [14] the relation between image quality and radiation dosage is non-linear. From the study [15] it can be inferred that the minimum number of incident photons varies as the cube of the number of pixels and the radiation dosage varies as the hypercube (fourth power) of the number of pixels. So, if the number of pixels is reduced to half, the radiation dosage reduces to one-sixteenth.

Efforts to Reduce X-Ray Radiation Exposure: X-ray machines have two main components - emitter and detector. The radiation exposure of the patient can be reduced by using lower emitted radiation or reducing the detection limit of the detector [16].

An early study from 1994 [17] suggests that radiation exposure for patients and doctors in fluoroscopic procedures can be reduced by making manual adjustments at the time of the procedure. The requirement of a particular radiation dosage has been found to be linked to the output image/video quality. At higher doses the images provide good and noise-free visualization and the dosage provided during a scan should follow the As Low As Reasonably Achievable (ALARA) principle. The study points out that the X-ray dose can be reduced if the detector is placed as close to the body as possible, to reduce the entrance radiation to the skin. The radiation emitted from the X-ray machine also contains some harmful low energy non-penetrating rays that are absorbed by the skin. For medical imaging, these radiations are absorbed by a filtering material made of aluminum. Appropriate filter thickness can be used to absorb the non-penetrating harmful X-rays before it penetrates the skin, causing irreversible damage. Pulsed fluoroscopy has been suggested as another way to reduce radiation, instead of continuous fluoroscopy. A later study [18] also emphasizes the use of additional filtration and pulsed fluoroscopy for patient dose reduction. They noticed that dose reduction was achieved by making use of digital zoom in place of magnifying the images. A study [19] demonstrated the use of monochromatic X-rays to reduce radiation exposure by 30%. Authors of the study [20] have successfully reduced the radiation by using a 4in x 5in x-ray film instead of the standard 14in x 17in film for diagnosing tuberculosis.

Interpretation of Chest X-Rays: All the above methods propose different ways of reducing the X-rays falling on the human body, while trying to retain a good resolution output image. The X-ray scan image is interpreted by expert doctors and radiologists. With learning and experience, they can diagnose the presence or absence of diseases from the scans. The advancement of deep learning techniques in image analysis has helped the medical industry to analyze medical images faster and with increasing accuracy. Various deep learning studies work towards aiding doctors in interpreting X-ray scans by predicting the disease based on previous learning. These deep learning models are found to be highly accurate with high levels of sensitivity and specificity. On the one hand, the resolution of X-ray has been improving with the advent of new technology, while on the other, deep learning and computer vision models have advanced and can find patterns in images which humans cannot. The power of machines is beyond interpreting the high dimension X-ray scans by humans. It is found to discover relevant patterns in low dimension scans which make no sense to the human eyes.

Detection of Covid-19 and Pneumonia using Chest X-rays: Many predictive deep learning models have been studied for Covid-19 and Pneumonia detection [26-30], but they focus on the model performance and not on the image size used for the study. These studies have used different image sizes ranging from 112 x 112 px to 800 x 800 px and reported a model performance ranging from 89.6% to 99.53%. Internet of Things has also been used

to check the spread of Covid-19 [31] with a detection algorithm using chest X-rays, particle swarm optimization and support vector machines to achieve competitive performance with lower computational power. Radiological scans have also been used for image segmentation using generative adversarial networks and gradient penalty Reference [32].

In this work, we try to find an optimal dimension of x-ray images in Covid-19 and Pneumonia disease diagnosis by navigating the trade-off between the image dimension and diagnostic power of a medical imaging strategy. Similar studies have been performed for breast cancer diagnosis [24] and lung disease diagnosis [25]. In cancer diagnosis on the data collected from two hospitals, the best performance for MobileNet model was at image size of 320 x 320 px and DenseNet121 performed best at image size 448 x 448 px. The study on lung disease diagnosis was performed on the publicly available chest radiograph dataset released by National Institutes of Health. Maximum performance was observed for image dimensions between 256 x 256 px and 448 x 448 px. The ResNet34 and DenseNet121 models were used for this study. Our study is novel as the effect or image size has not been previously studied for Covid-19 and Pneumonia diagnosis. The objective of our study is attained by collecting the data sets from public domain and images available at different dimensions and evaluating their progressive or decreasing predictive power to discriminate between images belonging to Covid-19, Pneumonia, and control data sets.

Our results indicate that 128 x 128 px size of images is sufficient to accurately classify Covid-19 versus Pneumonia and both Covid-19 and Pneumonia versus control cases. An increased dimension size does not lead to any significant gain in diagnostic accuracy of medical imaging. Further, we find that the high dimension images guided by human inspection are unnecessary for the machine learning based diagnosis because the latter can accurately capture patterns in images otherwise not visible to the naked eye and therefore provide accurate diagnosis when human expertise may fail. We believe that these results will help the medical practitioners to avoid indiscriminate use of high radiation in their diagnostic activities.

2. Methods

2.1. Dataset

Experiments have been performed on the following medical imaging dataset: Chest X-Ray Covid-19 and Pneumonia Dataset: (https://www.kaggle.com/datasets/prashant268/chest-xray-covid19-pneumonia)

It contains 6432 x-ray images of Covid-19, Pneumonia and Normal cases. The dataset consists of training and test images. A validation set of 20% training data, has been created for fine tuning the model and 80% of the training data is used for training the model.

Table 1: Description of the dataset

Class	Total Number of Images	Training Images	Validation Images	Test Images
Covid-19	576	345	116	116
Pneumonia	4273	2563	855	855
Normal	1583	949	317	317

2.2. Data Preprocessing and Handling Data Imbalance

Images from all the three classes - Covid-19, Pneumonia and Normal have been first converted into 3-channel grayscale images. The images have been converted from rectangular to square images. The smaller side of the rectangle is considered and the longer side is cropped equally from the two ends to retain the meaningful lung area at the center. This will help to unify the aspect ratio while performing the experiment. Table 1 shows a high class-imbalance in the data. To address this the minority class samples have been randomly under sampled, to generate a balanced dataset. This balanced dataset has been generated by randomly sampling images from the larger datasets. To avoid bias in results due to random sampling, the average results of three randomly under sampled datasets have been reported.

2.3. Deep Learning Model

To train the images, EfficientNet B0 21 CNN model has been used. It is a light model with 11M trainable parameters. The 3-class problem has been divided into three binary classification problems.

Binary Classification 1: Covid-19 vs Normal;

Binary Classification 2: Covid-19 vs Pneumonia;

Binary Classification 3: Pneumonia vs Normal.

For each classification problem, the model is trained using transfer learning with pre-trained weights of the ImageNet dataset 22. The base model of EfficientNet B0 is accompanied by a fully connected layer with 512 nodes, Relu activation and 20% dropout. This is followed by an output layer with 3 nodes and softmax activation. The model is compiled using categorical cross-entropy loss function and Adam optimizer with an adaptive learning rate starting at 3e-5, to avoid overfitting of the model. Early stopping is used to stop training the model when the loss does not improve for 5 epochs. The model is evaluated on the test data and the metrics calculated for each classification problem are: Accuracy, AUC, F1 score and Matthews Correlation Coefficient (MCC).

2.4. Experimental Setup

All experiments have been performed on Kaggle using python programming language and the processing

resources of Kaggle. The EfficientNet B0 model was downloaded from Tensorflow hub. To perform the experiments, the batch size was set as 32. Image sizes used in the study are: 1 x 1, 2 x 2, 4 x 4, 8 x 8, 16 x 16, 32 x 32, 64 x 64, 128 x 128, 224 x 224, 256 x 256 and 300 x 300 pixels. Figure 1 shows the process flow followed in the study.

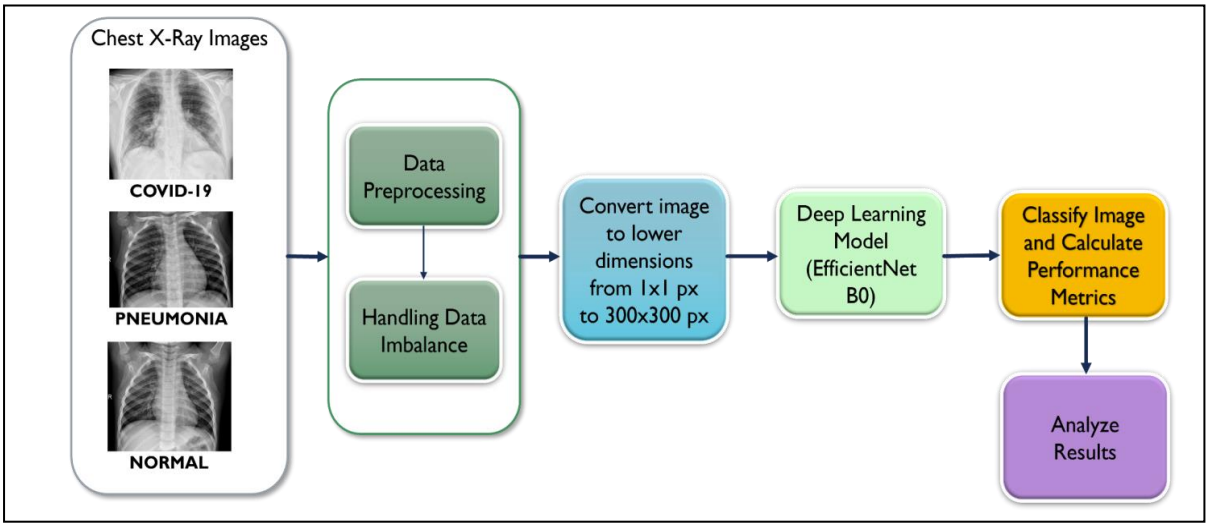

Figure 1: Process Flow

2.5. Disease Detection using rescaled X-rays at lower dimensions

The existing studies on detecting Covid-19 and Pneumonia using chest X-ray images work around reducing the original image size to various lower dimensions ranging from 112 to 800 (Figure 2). Most of the papers reduce the size to 224 x 224 px. In this study we try to see the effect of image size used in the model, by reducing the size from 300 x 300 px up to the trivial 1 x 1 px. The image sizes used in the study are: 1 x 1, 2 x 2, 4 x 4, 8 x 8, 16 x 16, 32 x 32, 64 x 64, 128 x 128, 224 x 224, 256 x 256 and 300 x 300 pixels. It can be seen from Figure 3 that as the image size decreases, the information visible to the human eye also reduces, but we find that machines can model images at lower dimensions also. The first question which arises here is, which X-ray dimension can be used for effective detection of the disease. The second question is, if images at lower dimensions are able to detect the disease, then can we collect X-rays at lower dimensions and further reduce the radiation exposure of patients. We try to highlight the radiation exposure vs detection performance for different image sizes based on the exposure-performance tradeoff.

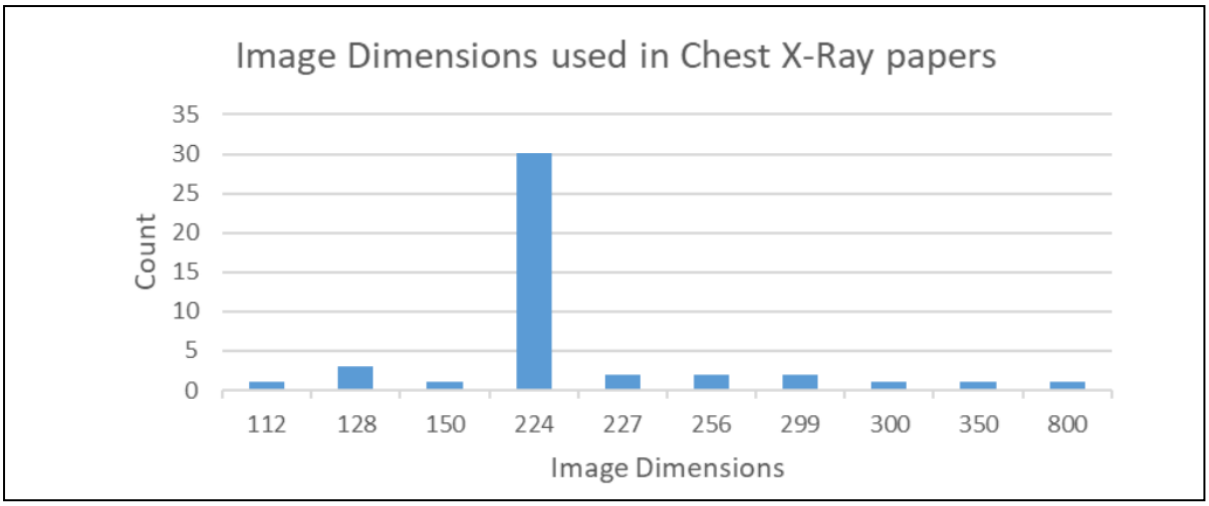

Figure 2: Image sizes used by models in 44 research publications reviewed for this study [Detailed references can be found in Supplementary data]

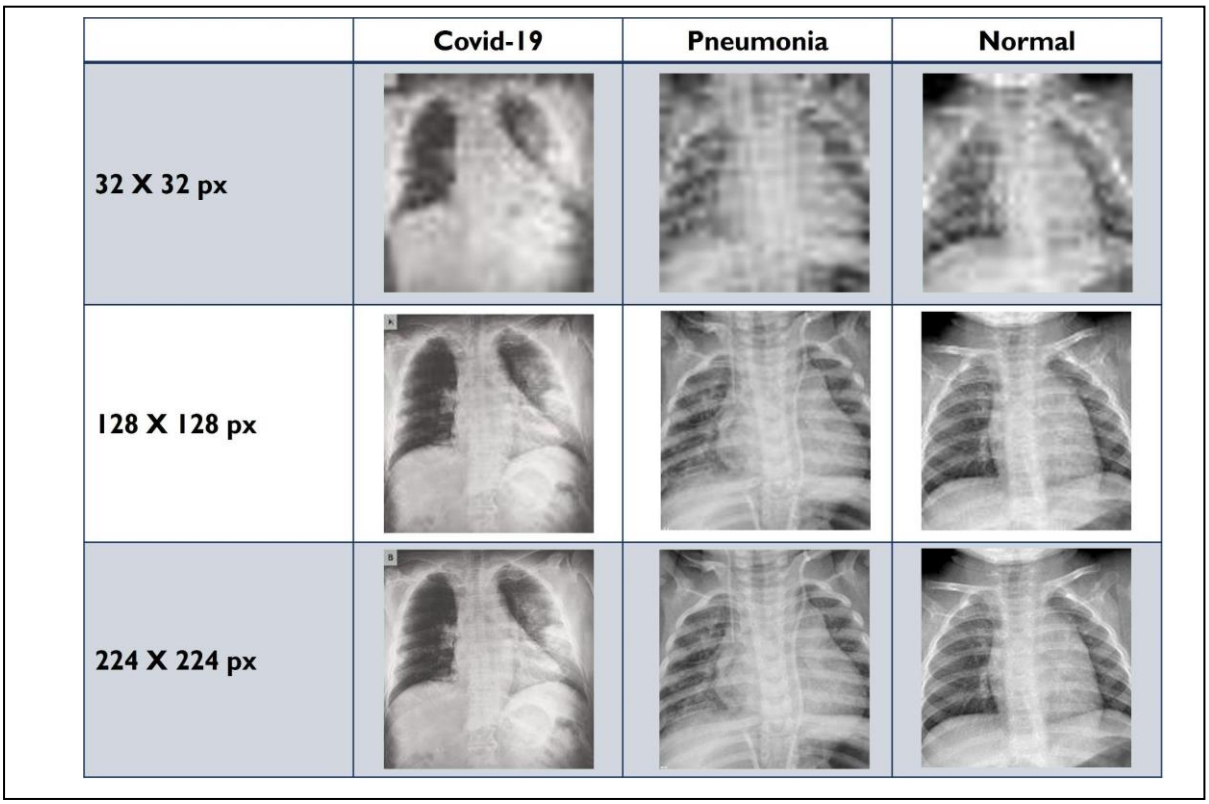

Figure 3: Visualizing images reduced to lower dimensions: 32 x 32 px, 128 x 128 px and 224 x 224 px

2.6. Generating Higher Dimension images from Low Dimension X-ray scans

We have low dimension images and deep learning models which predict the diseases from chest X-rays, but the final decision in the medical field is always in the hands of the medical practitioner. To bridge this gap, higher dimension images have been regenerated from the low dimensional X-rays for better visualizations, using SRGAN (Super-Resolution Generative Adversarial Network) [23]. It is a combination of a generator network and a discriminator network, which work together to generate high-dimensional images from low-dimensional input. SRGAN is capable of producing realistic images, with a high level of detail and sharpness. This higher

dimension image, in combination with the results of the model using low dimension x-ray scans can prove beneficial to the patients and the doctors.

3. Results

3.1. Prediction of disease from low-dimension X-rays

Three Binary Classification problems have been used in this study: Covid-19 vs Normal; Covid-19 vs Pneumonia and Pneumonia vs Normal. Table 2 shows the performance scores for all image sizes in the study. Overall, negligible learning has been observed from 1 x 1 to 4 x 4 px image size. Learning is seen to pick up from 8 x 8 px size and increase with image size up to 128 x 128 px. In all the three binary classification problems, there is very little increase in performance from 128 x 128 to 300 x 300 px.

In the Covid-19 vs Normal classification, the AUC on test data [Table 2] for image size 128 x 128 px is 99.94% while it is 99.97%, 99.98% and 100% for image sizes 224 x 224, 256 x 256 and 300 x 300 px respectively. For a lower image size of 64 x 64 px, the AUC score is 95.35%. The model records an almost consistent performance for image sizes starting from 128 x 128 px. For the second task of detecting Covid-19 vs Pneumonia, AUC score of 99.54% has been observed for image size 128 x 128 px and this increases to 99.94%, 99.98% and 99.97% for image sizes 224 x 224, 256 x 256 and 300 x 300 px. So, a slight drop in performance from 256 x 256 px to 300 x 300 px is noticed. For the third classification task between Pneumonia and Normal cases, performance scores are slightly lower. The test AUC at 128 x 128 px is 97.99% and the AUC scores are 98.03%, 98.8% and 99.05% at image sizes 224 x 224, 256 x 256, and 300 x 300 px.

3.2. Reduction in radiation dosage by using low-dimension X-rays

From Figure 2 it can be seen that around 32 out of 44 reviewed papers have reduced the image size to 224 x 224 px for their study. From our study, we find that the AUC scores increase by 0.03%, 0.5% and 0.04% from 128 x 128 px to 224 x 224 px in our three classification tasks respectively. From the confusion matrices for 128 x 128 px and 224 x 224 px in Figure 6, we can infer that there is a slight improvement in the number of correct classifications, from 128 x 128 px to 224 x 224 px.

The Radiation Dosage and Test AUC score plot in Figure 4 further validates our argument of slight improvement in model performance vs large increase in radiation dosage from X-ray image size 128 x 128 px onwards. To achieve this small increase in performance, we expose the patient to around 9 times more radiation. If the image size is increased to 300 x 300 px, the radiation dosage comparatively increases by around 30 times.

The actual image sizes in the dataset range from around 800 x 800 px to 2000 x 2000 px with an average size of around 1000 x 1000 px.

At the image size of 1000 x 1000 px, the radiation dosage is 3,725 times as compared to the dosage for 128 x 128 px image and around 400 times more than the radiation dosage if the X-ray image size is 224 x 224 px.

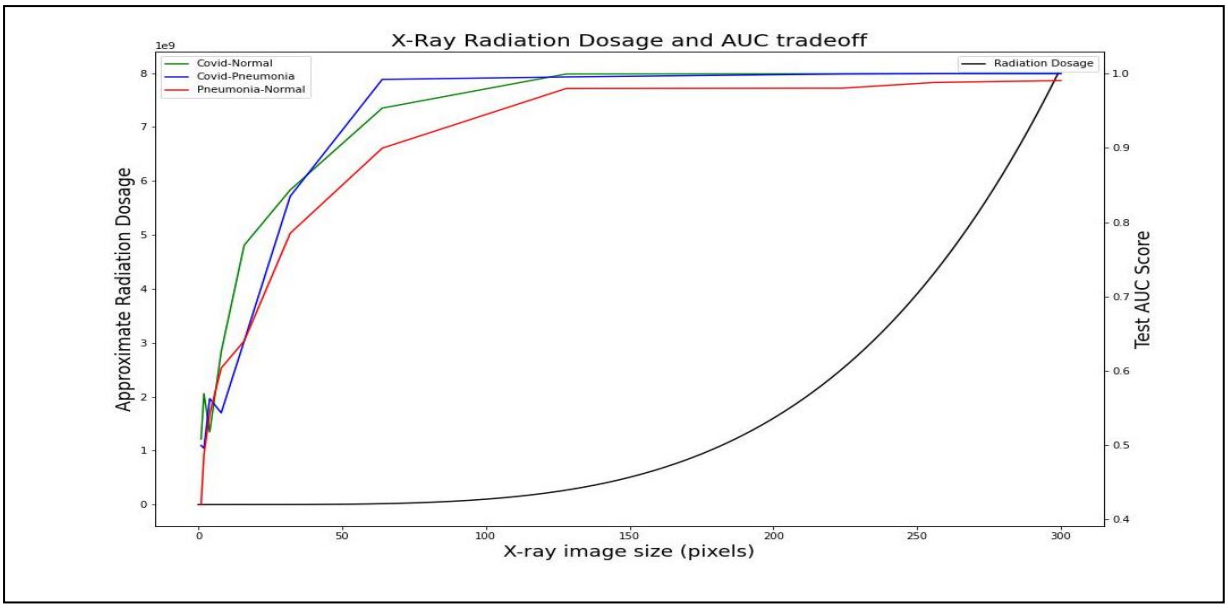

Figure 4: Radiation Dosage-Performance tradeoff for different image sizes

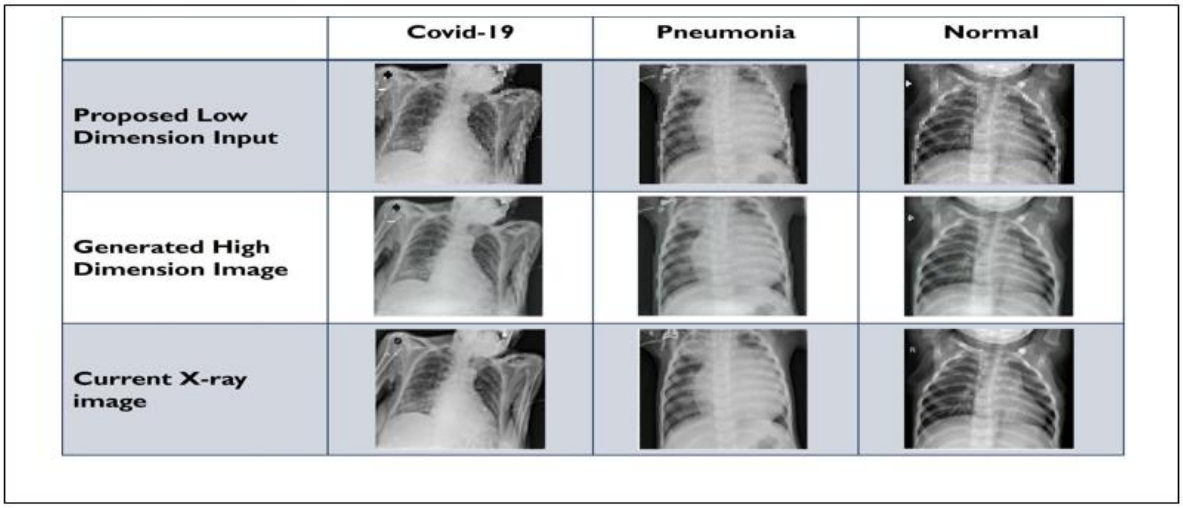

Figure 5: Proposed Low Dimension X-ray images, Generated High Dimension X-ray images from the low dimension input using SRGAN and Current images in the dataset

Table 2: Performance Metrics for images at different X-Ray image sizes

	Metrics (%)	Image Size (pixels)										
		1x1	2x2	4x4	8x8	16x16	32x32	64x64	128x128	224x224	256x256	300x300
Covid-19 vs Normal	Accuracy	50.14	53.16	52.44	56.47	70.55	76.29	89.94	98.99	98.99	99.71	100
	AUC	**50.81**	**56.95**	**51.78**	**62.58**	**76.91**	**84.34**	**95.35**	**99.94**	**99.97**	**99.98**	**100**
	F-score	48.18	50.52	50.65	55.47	65.89	73.83	85.42	98.7	99.09	99.74	100
	MCC	-3.65	1.04	1.3	10.94	31.77	47.66	70.83	97.4	98.18	99.48	100
Covid-19 vs Pneumonia	Accuracy	51.87	49.71	53.88	52.73	60.49	75.72	95.83	97.84	99.57	99.43	99.71
	AUC	**49.97**	**49.58**	**56.27**	**54.35**	**64.02**	**83.49**	**99.21**	**99.54**	**99.94**	**99.98**	**99.97**
	F-score	49.74	48.57	53.52	48.96	58.72	76.04	96.22	98.05	99.61	99.48	99.74
	MCC	-0.52	-2.86	7.03	-2.08	17.45	52.08	92.45	96.09	99.22	98.96	99.48
Pneumonia vs Normal	Accuracy	49.86	49.43	51.87	54.89	58.62	70.4	81.03	93.1	94.25	94.83	95.4
	AUC	**42.01**	**48.74**	**54.23**	**60.37**	**64.03**	**78.51**	**89.96**	**97.99**	**98.03**	**98.8**	**99.05**
	F-score	48.31	48.31	53.26	58.33	58.98	70.83	82.03	93.75	94.79	95.31	95.83
	MCC	-3.39	-3.39	6.51	16.67	17.97	41.67	64.06	87.5	89.58	90.62	91.67

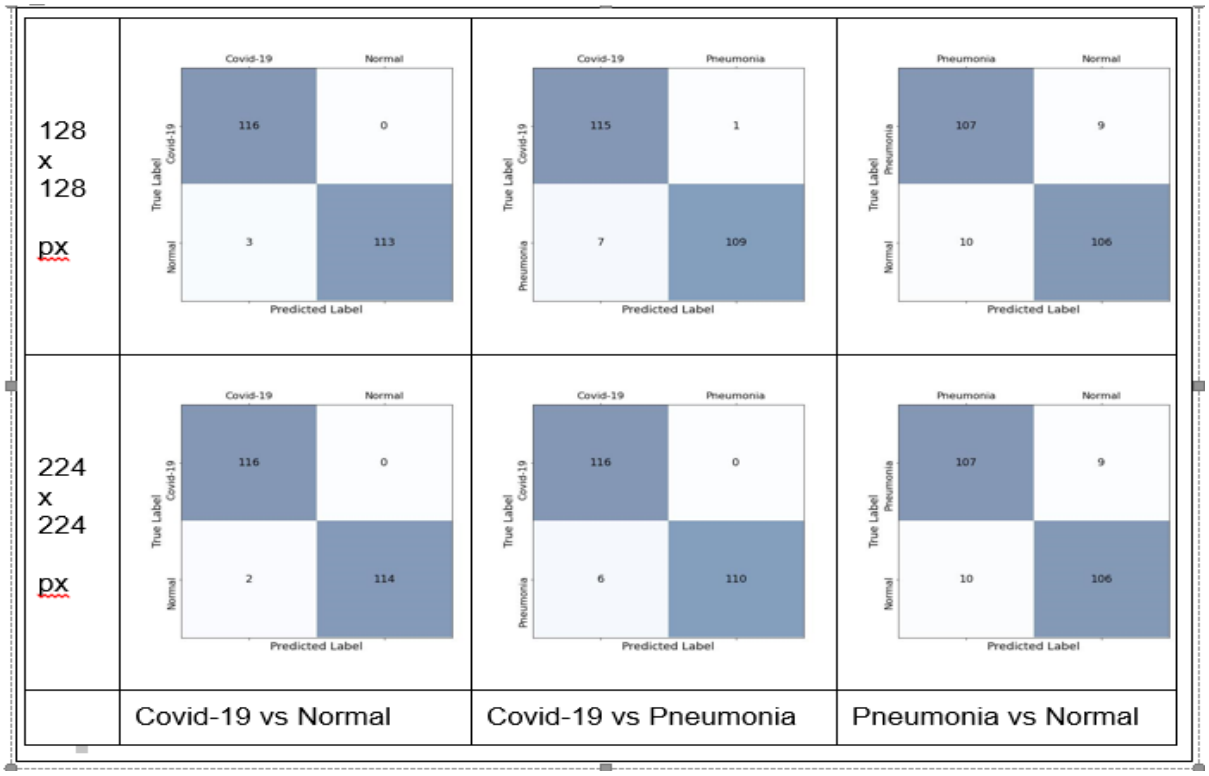

Figure 6: Confusion Matrix for image size 128 x 128 px and 224 x 224 px for all three binary classification problems

4. Discussion

Chest X-rays are one of the simplest radiographic diagnostic procedures involving much less radiation exposure as compared to other more complex procedures like Computer Tomography (CT) and Fluoroscopic Angiography, among others. If the radiation exposure in chest X-rays can be further reduced, other procedures can follow similar methodology and achieve reduction in radiation exposure. It is also observed that the quality of images becomes poor to the naked eye while the machine learning models continue to perform well, suggesting that we should employ different standards of image sizes for human versus machine-based automated diagnosis. This does not mean two sets of X-rays have to be generated for a clinical purpose. In fact, many super-resolution techniques have now been developed and future work may look at the ability to produce images that can be suitable for the human eye to interpret from those collected at low dimensions from image sources. So, to give a high dimension X-ray image to the doctors and patients, we also propose to generate high dimension images from the low dimension input images using Generative Adversarial Network (GAN) as seen in Figure 5.

The EfficientNetB0 model has been used in this study to train the datasets. Starting from lower image sizes, good model performance is noticed at 128 x 128 px and only slight improvement is noticed in higher sizes. On the other hand, when the image size increases from 128 x 128 px to 224 x 224 px, the radiation exposure to the patient increases by around 9 times, whereas when we compare it with the average size of the original images in the dataset (1000 x 1000 px), the radiation dosage is found to increase by a factor of 3,725. A balance between

model performance and radiation exposure of the patients' needs to be maintained. We call this the Radiation Exposure-Performance tradeoff.

Similar study has been performed for breast cancer and lung disease diagnosis suggesting an image size of 320 x 320 px and 480 x 480 px for different deep learning models. In the realm of chest x-rays, no such study has been performed earlier.

5. Conclusion

From this study it is evident that deep learning models are able to learn effectively from low dimension chest X-ray images, where the human eye fails. The advancement in the field of artificial intelligence can be used to the benefit of patients by reducing the size of the x-ray images captured. This in turn will reduce radiation exposure manifold. To generate a higher dimension image for the medical practitioners, we suggest using generative models like Generative Adversarial Networks (GAN). In this way, both patients and doctors will be in a win-win situation - exposure reduction for patients and high dimension scans for inspection by doctors and radiologists.

The size of X-ray images collected from patients and their radiation exposure can be reduced and an informed decision based on the exposure-performance tradeoff can be taken by the doctors and patients on a case-to-case basis. Due to its general design, we believe this study can be extended to other methods that make use of X-rays or other high intensity radiation for medical diagnosis.

6. Caveats and Limitations of the study

One caveat in this study is that the low dimension images have been generated from the ones which were originally high dimension images. There is a possibility that the dimensionality reduction of images may leak some of the information into lower dimensions, which would not be collected by images recorded at lower dimensions in the clinical settings. This question cannot be settled within the scope of this paper as a thorough investigation of this will require simultaneous collection of images at low and high dimensions. However, the results presented here encourage further clinical validation of these outcomes. The promise of reducing radiation exposure by thousands is a strong motivation to do so.

Another limitation of this study is that it has been performed on one deep learning model. The results can be generalized by extending the study to other deep learning models.

7. Declarations

Ethics approval and consent to participate: Not Applicable

Consent for publication: Not Applicable

Availability of data and materials: The datasets analyzed during the current study are available in the Kaggle

repository: https://www.kaggle.com/datasets/prashant268/chest-xray-covid19-pneumonia

Competing interests: The authors declare that they have no competing interests

Authors' contributions: DP wrote the codes for the experiment and preprocessed the image dataset. NV executed the code, analyzed results and prepared the draft paper along with visualizations. SA conceptualized the study, coordinated the work and reviewed and edited the paper.

Acknowledgements: This study was supported in part by DBT bioinformatics center funded to SCIS, JNU, DBT-NNP funded in collaboration to JNU and ICMR project on "Artificial Intelligence and Machine Learning methods for drug resistance of Tuberculosis in India" vide grant number Al-Adhoc/12/2022-AI Cell funded to SA.

References

[1]. Morgan W. XIV. Electrical experiments made in order to ascertain the non-conducting power of a perfect vacuum. Philosophical Transactions of the Royal Society of London. 1785 Dec 31(75):272-8.

[2]. Anderson JG. William Morgan and X-rays. Transactions of the Faculty of Actuaries. 1945 Jan;17:219-21.

[3]. Zhou Y, Yang L, Han M, Huang M, Sun X, Zheng W, Han W, Wang J. Case report on early diagnosis of COVID-19. Disaster Medicine and Public Health Preparedness. 2020 Dec;14(6):e22-5.

[4]. Wall BF, Kendall GM, Edwards AA, Bouffler S, Muirhead CR, Meara JR. What are the risks from medical X-rays and other low dose radiation?. The British journal of radiology. 2006 Apr 1;79(940):285-94.

[5]. Zamanian A, Hardiman CJ. Electromagnetic radiation and human health: A review of sources and effects. High Frequency Electronics. 2005 Jul 20;4(3):16-26.

[6]. Brenner DJ, Hall EJ. Computed tomography—an increasing source of radiation exposure. New England journal of medicine. 2007 Nov 29;357(22):2277-84.

[7]. Luan FJ, Wan Y, Mak KC, Ma CJ, Wang HQ. Cancer and mortality risks of patients with scoliosis from radiation exposure: a systematic review and meta-analysis. European Spine Journal. 2020 Dec;29:3123-34.

[8]. Gislason-Lee AJ. Patient X-ray exposure and ALARA in the neonatal intensive care unit: global patterns. Pediatrics & Neonatology. 2021 Jan 1;62(1):3-10.

[9]. Arad I, Simanovsky N, Braunstein R. Exposure of extremely low birth weight infants to diagnostic X-Rays: a longitudinal study. Acta Paediatrica. 2009 Feb;98(2):266-9.

[10]. Rudan I, Boschi-Pinto C, Biloglav Z, Mulholland K, Campbell H. Epidemiology and etiology of childhood pneumonia. Bulletin of the world health organization. 2008;86:408-16B.

[11]. Hendrick RE. Radiation doses and risks in breast screening. Journal of Breast Imaging. 2020 May;2(3):188-200.

[12]. Smith-Bindman R, Lipson J, Marcus R, Kim KP, Mahesh M, Gould R, De González AB, Miglioretti DL. Radiation dose associated with common computed tomography examinations and the associated

lifetime attributable risk of cancer. Archives of internal medicine. 2009 Dec 14;169(22):2078-86.

[13]. Rubai SS, Rahman MS, Purohit S, Patwary MK, Moinul AK, Meaze H, Mamun AA. Measurements of entrance surface dose and effective dose of patients in diagnostic radiography. Biomedical Journal. 2018;1:5.

[14]. Barrett HH, Myers KJ, Hoeschen C, Kupinski MA, Little MP. Task-based measures of image quality and their relation to radiation dose and patient risk. Physics in Medicine & Biology. 2015 Jan 7;60(2):R1.

[15]. Grodzins L. Optimum energies for x-ray transmission tomography of small samples: Applications of synchrotron radiation to computerized tomography I. Nuclear Instruments and Methods in Physics Research. 1983 Mar 1;206(3):541-5.

[16]. Brenner DJ, Elliston CD, Hall EJ, Berdon WE. Estimated risks of radiation-induced fatal cancer from pediatric CT. American journal of roentgenology. 2001 Feb;176(2):289-96.

[17]. Wagner LK, Eifel PJ, Geise RA. Potential biological effects following high X-ray dose interventional procedures. Journal of Vascular and Interventional Radiology. 1994 Jan 1;5(1):71-84.

[18]. Geleijns J, Wondergem J. X-ray imaging and the skin: radiation biology, patient dosimetry and observed effects. Radiation protection dosimetry. 2005 May 17;114(1-3):121-5.

[19]. Cherepennikov Y, Gogolev A. Method to reduce radiation exposure in the medical X-ray diagnostics. In2012 7th International Forum on Strategic Technology (IFOST) 2012 Sep 18 (pp. 1-5). IEEE.

[20]. Douglas BH, Birkelo CC, Harmon GE, Vaughan HF. Use of Miniature X-Ray Films in Tuberculosis Case Finding. American Journal of Public Health and the Nations Health. 1940 Dec;30(12):1427-30.

[21]. Tan M, Le Q. Efficientnet: Rethinking model scaling for convolutional neural networks. InInternational conference on machine learning 2019 May 24 (pp. 6105-6114). PMLR.

[22]. Deng J, Dong W, Socher R, Li LJ, Li K, Fei-Fei L. ImageNet: A large-scale hierarchical image database. In2009 IEEE conference on computer vision and pattern recognition 2009 Jun 20 (pp. 248-255). Ieee.

[23]. Ledig C, Theis L, Huszár F, Caballero J, Cunningham A, Acosta A, Aitken A, Tejani A, Totz J, Wang Z, Shi W. Photo-realistic single image super-resolution using a generative adversarial network. InProceedings of the IEEE conference on computer vision and pattern recognition 2017 (pp. 4681-4690).

[24]. Tang S, Jing C, Jiang Y, Yang K, Huang Z, Wu H, Cui C, Shi S, Ye X, Tian H, Song D. The effect of image resolution on convolutional neural networks in breast ultrasound. Heliyon. 2023 Aug 1;9(8).

[25]. Sabottke CF, Spieler BM. The effect of image resolution on deep learning in radiography. Radiology: Artificial Intelligence. 2020 Jan 22;2(1):e190015.

[26]. Afshar P, Heidarian S, Naderkhani F, Oikonomou A, Plataniotis KN, Mohammadi A. Covid-caps: A capsule network-based framework for identification of covid-19 cases from x-ray images. Pattern Recognition Letters. 2020 Oct 1;138:638-43.

[27]. Al-Waisy AS, Al-Fahdawi S, Mohammed MA, Abdulkareem KH, Mostafa SA, Maashi MS, Arif M, Garcia-Zapirain B. COVID-CheXNet: hybrid deep learning framework for identifying COVID-19 virus in chest X-rays images. Soft computing. 2023;27(5):2657.

[28]. Gupta A, Gupta S, Katarya R. InstaCovNet-19: A deep learning classification model for the detection

of COVID-19 patients using Chest X-ray. Applied Soft Computing. 2021 Feb 1;99:106859.

[29]. Heidari M, Mirniaharikandehei S, Khuzani AZ, Danala G, Qiu Y, Zheng B. Improving the performance of CNN to predict the likelihood of COVID-19 using chest X-ray images with preprocessing algorithms. International journal of medical informatics. 2020 Dec 1;144:104284.

[30]. Minaee S, Kafieh R, Sonka M, Yazdani S, Soufi GJ. Deep-COVID: Predicting COVID-19 from chest X-ray images using deep transfer learning. Medical image analysis. 2020 Oct 1;65:101794.

[31]. Shen C, Zhang K, Tang J. A covid-19 detection algorithm using deep features and discrete social learning particle swarm optimization for edge computing devices. ACM Transactions on Internet Technology (TOIT). 2021 Dec 30;22(3):1-7

[32]. He J, Zhu Q, Zhang K, Yu P, Tang J. An evolvable adversarial network with gradient penalty for COVID-19 infection segmentation. Applied Soft Computing. 2021 Dec 1;113:107947.